Future Reductions in Polar Cold Air Mass and Cold Air Outbreaks Revealed From Isentropic Analysis

doi: 10.1029/2019GL086076

Geophysical Research Letters

RESEARCH LETTER
10.1029/2019GL086076

Future Reductions in Polar Cold Air Mass and Cold Air Outbreaks Revealed From Isentropic Analysis

Yuki Kanno[1] and Toshiki Iwasaki[2]

[1]Institute for Space-Earth Environmental Research, Nagoya University, Nagoya, Japan, [2]Department of Geophysics, Graduate School of Science, Tohoku University, Sendai, Japan

Key Points:
- Under the RCP8.5 scenario, the polar cold air mass is projected to decrease by 37% in the boreal winter by the end of 21st century
- The equatorward polar cold air mass fluxes in the midlatitudes are projected to decrease significantly by around 2050
- Thermodynamical (dynamical) change is the main (secondary) contributor to the projected reduction in the polar cold air mass fluxes

Supporting Information:
- Supporting Information S1

Correspondence to:
Y. Kanno,
kanno@isee.nagoya-u.ac.jp

Citation:
Kanno, Y., & Iwasaki, T. (2020). Future reductions in polar cold air mass and cold air outbreaks revealed from isentropic analysis. *Geophysical Research Letters*, *47*, e2019GL086076. https://doi.org/10.1029/2019GL086076

Received 1 NOV 2019
Accepted 9 DEC 2019
Accepted article online 11 DEC 2019

Abstract This study quantifies future changes in the polar cold air mass (PCAM) below a threshold potential temperature of 280 K and its horizontal fluxes, which are an indicator for the intensity of cold air outbreaks, by analyzing the outputs from five climate models from the Fifth Coupled Model Intercomparison Project. Under the business-as-usual scenario, the multimodel means of the wintertime total hemispheric PCAM decrease by 37% in the Northern Hemisphere and by 34% in the Southern Hemisphere by the end of the 21st century. The midlatitude equatorward PCAM fluxes are projected to decrease significantly by around 2050. This is primarily due to the reduction of the PCAM and to a lesser extent due to the weakening of the extratropical meridional circulation. Finally, intermodel differences in the total hemispheric PCAM reduction are shown to be linearly related to the climate sensitivity to the global mean surface air temperature.

Plain Language Summary In winter, the polar regions are reservoirs of extremely cold air masses. Sometimes, the polar cold air outflows to the midlatitudes and results in very cold weather. This study quantitatively evaluated the future changes in the polar cold air mass and its outflow to the midlatitudes in the winter hemispheres. We found that both the polar cold air mass and its outflow are projected to decrease significantly by the end of the 21st century in the Northern and Southern Hemispheres due to the increase in the global mean surface temperature. These findings provide a possible scenario of future polar climate change.

1. Introduction

The polar regions have experienced drastic climate change in recent decades. In the Arctic, the surface air temperature has been increasing almost twice as fast as the global mean, and this is known as Arctic amplification (Bekryaev et al., 2010; Screen & Simmonds, 2010; Serreze et al., 2009). Analyses of atmospheric reanalysis data sets and observational data showed that the volume of cold air has decreased significantly in the high latitudes of the Northern Hemisphere (NH) winter since the 1960s (Hankes & Walsh, 2011; Martin, 2015). In the Southern Hemisphere (SH) winter, strong warming has been observed in the western part of Antarctica, especially over the Antarctic Peninsula (Steig et al., 2009). Climate model experiments have projected future warming in the Arctic regions (Holland & Bitz, 2003; Kay et al., 2012), but there are large discrepancies in the magnitude of increase (IPCC, 2013). In addition, the mechanisms for future changes in the Antarctic temperature are not fully understood yet.

Cold air outbreaks (CAOs) are intermittent outflows of cold air from polar regions to the midlatitudes. They are characterized by a sudden temperature drop, a strong northerly wind, and abrupt pressure increase (e.g., Zhang et al., 1997). CAOs are one of the most vigorous weather phenomena in the winter extratropics and cause tremendous damage to society through low temperatures and heavy snowfall. However, they are projected to be less severe in future climates (Ayarzagüena & Screen, 2016; Gao et al., 2015; Kodra et al., 2011; Landgren et al., 2019; Park et al., 2011; Peings et al., 2012; Vavrus et al., 2006). Their intensity and/or frequency are projected to decrease significantly. However, most previous studies cited above have used only surface air temperature to detect CAO events and have not explicitly evaluated the transport of cold air.

Isentropic definitions of the amount of cold air and its horizontal fluxes facilitate a quantitative understanding of polar warming and CAO activity (Iwasaki et al., 2014; Kanno et al., 2016; Kanno et al., 2019; Sasai et al., 2019; Shoji et al., 2014). Kanno et al. (2016) studied long-term trends in the polar cold air mass

(PCAM) below a threshold potential temperature of 280 K and its horizontal fluxes by using several atmospheric reanalysis data sets. They showed that the total hemispheric PCAM has been reducing at a rate of about 1.0% per decade in the NH winter over the period from 1980 to 2012, whereas Abdillah et al. (2018) showed that its internal variability is dominated by the El Niño and Southern Oscillation. No significant long-term trends in the equatorward PCAM fluxes across 45°N, in contrast to the total PCAM, were found due to their large internal variability. In the SH winter, linear trends cannot be observed due to large discrepancies in linear trends between reanalysis data sets. This study quantifies future changes in the winter season using data from multiple climate models forced by two future projection scenarios from the Coupled Model Intercomparison Project Phase 5 (CMIP5) archives.

2. Data and Method

2.1. Data

This study has used the output from five climate models CanESM2, GFDL-CM3, HadGEM2-ES, MIROC5, and MRI-CGCM3 from the CMIP5 archives (Taylor et al., 2012) because they have the highest spatial and vertical resolutions among the 14 CMIP5 models that provide six-hourly model level data. We use three long-term experiments: the historical and Representative Concentration Pathway (RCP) 4.5 and 8.5 scenarios. The RCP4.5 scenario represents a midrange mitigation emission scenario, whereas the RCP8.5 scenario represents a high emission scenario and is called the business-as-usual scenario. We analyzed the projected changes in the RCP4.5 and 8.5 experiments in the mid- and late 21st century (2046–2065 and 2081–2100, respectively) relative to the historical scenario under the present climate (1981–2000). Because the RCP4.5 and 8.5 experiments in HadGEM2-ES end on the last day of December 2099, the period of the late 21st century in this model is limited to 19 years: from 2081 to 2099. The analyses here focus only on the winter seasons: December–February for the NH and June–August for the SH.

2.2. Definition of PCAM Amount, PCAM Fluxes, and Negative Heat Content

The definition of PCAM amount follows Iwasaki et al. (2014). The PCAM amount, PCAM flux, and negative heat content (NHC) are defined as follows:

$$\text{PCAM amount} \equiv p_s - p(\theta_T), \tag{1}$$

$$\textbf{PCAM flux} \equiv \int_{p(\theta_T)}^{p_s} \mathbf{v}\, dp, \tag{2}$$

$$\text{NHC} \equiv \int_{p(\theta_T)}^{p_s} (\theta_T - \theta)\, dp, \tag{3}$$

where p_s is surface pressure, p is pressure, θ_T is the threshold potential temperature, and $\mathbf{v}$ is the horizontal wind vector. The threshold potential temperature is set to 280 K. The total hemispheric PCAM amount (NHC) is computed as the spatial integration of the PCAM amount (NHC) in the winter hemisphere divided by the gravitational acceleration (Kanno, Shoji, et al., 2015). The zonal integration of the equatorward PCAM fluxes at 45°N and 50°S indicates the CAO activity for the NH and SH winters, respectively, and at 45°N within 90°E–135°E and at 60°N within 80°W–130°W measures the CAO activity over East Asia and North America, respectively (Kanno et al., 2017; Shoji et al., 2014). PCAM amount, PCAM flux, and NHC are computed from the six-hourly model level data after interpolation onto 2.5° × 2.5°grid, and they are then averaged over the present or future periods. We confirmed that the five selected climate models reproduce the climatological means of the total hemispheric PCAM amount in the winter hemispheres well (Supporting Information Figure S1).

For the future changes in the PCAM fluxes, adjustments of the threshold potential temperature should be considered. In this study, in addition to the future changes in the PCAM flux below 280 K, we also evaluate the future changes in the intensity of the extratropical direct (ETD) circulation, which is equivalent to the PCAM flux with an adjusted threshold potential temperature. The intensity of the ETD circulation is estimated by the isentropic mass-stream function χ, calculated as follows:

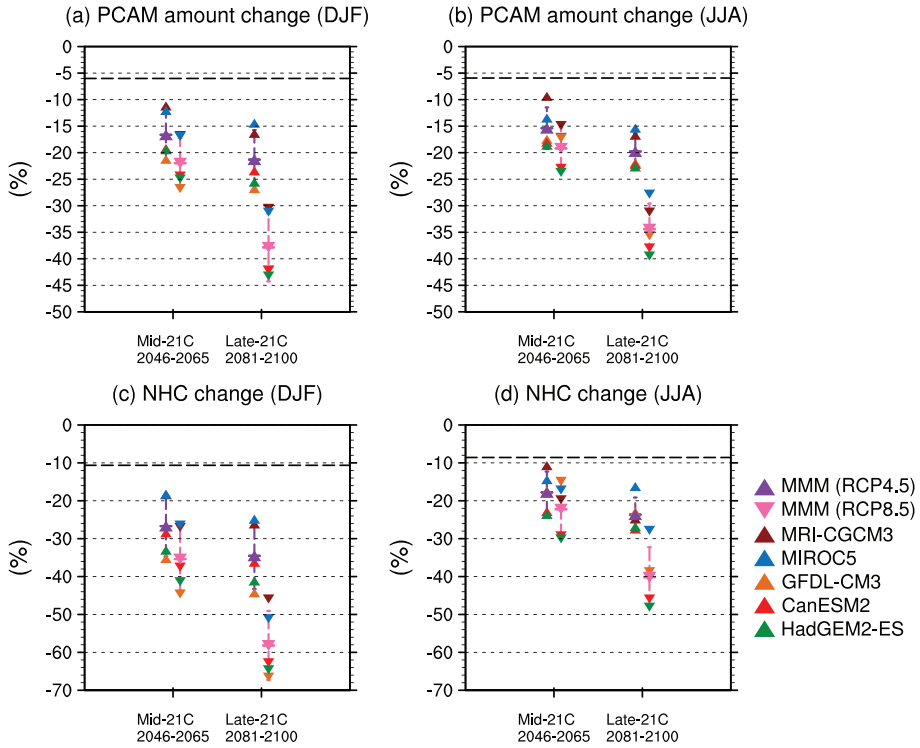

Figure 1. Future changes in the total hemispheric polar cold air mass (PCAM) amount (upper panels) and negative heat content (NHC) (lower panels). Future changes are relative to the present climate (1981–2000). Filled triangles indicate that changes are statistically significant at the 95% confidence level for each climate model and that changes satisfy the "large change with high model agreement" criteria for the multimodel mean. Purple and pink vertical bars represent the widths of the distributions (one standard deviation of the intermodel variability). Black bold broken horizontal lines denote the internal variability (two standard deviations of the interannual variability).

$$\chi(\phi,\theta) = -\frac{2\pi a\cos\phi}{g}\int_0^{2\pi}\int_\theta^\infty v\ \sigma d\ \theta d\ \lambda, \tag{4}$$

where λ is longitude, ϕ is latitude, g is gravitational acceleration, a is the radius of the Earth, v is the meridional wind, and $\sigma \equiv -\frac{1}{g}\frac{\partial p}{\partial \theta}$ is the density in isentropic coordinates. The intensity of the ETD circulation is estimated from the maximum (minimum) value of the mass-stream function in the extratropics (poleward of 30°N/S) in the NH (SH) winter. It is evaluated for each year and then averaged over the present or future periods, so interannual changes in the maximum (minimum) values and positions of the ETD circulation can be considered.

2.3. Statistical Significance

The statistical significance is tested by a two-tailed Student's *t* test at the 95% confidence level. If the projected change in the multimodel mean is larger than the internal variability, defined as two standard deviations of the interannual variability in the present climate averaged over the five climate models, and 80% of the climate models have the same sign as the changes in the multimodel mean, the result is consider to be a "large change with high model agreement."

3. Results

Figure 1 shows the projected changes in the total hemispheric PCAM amount and NHC under the RCP4.5 and 8.5 scenarios in the mid- and late 21st century relative to the present climate. The climatological mean distributions of the PCAM amount and NHC are shown in Figure S2. All five climate models project that the total hemispheric PCAM amount and NHC decrease in both the NH and SH winters in the future. All changes satisfy the "large change with high model agreement" criteria, indicating the robustness of the

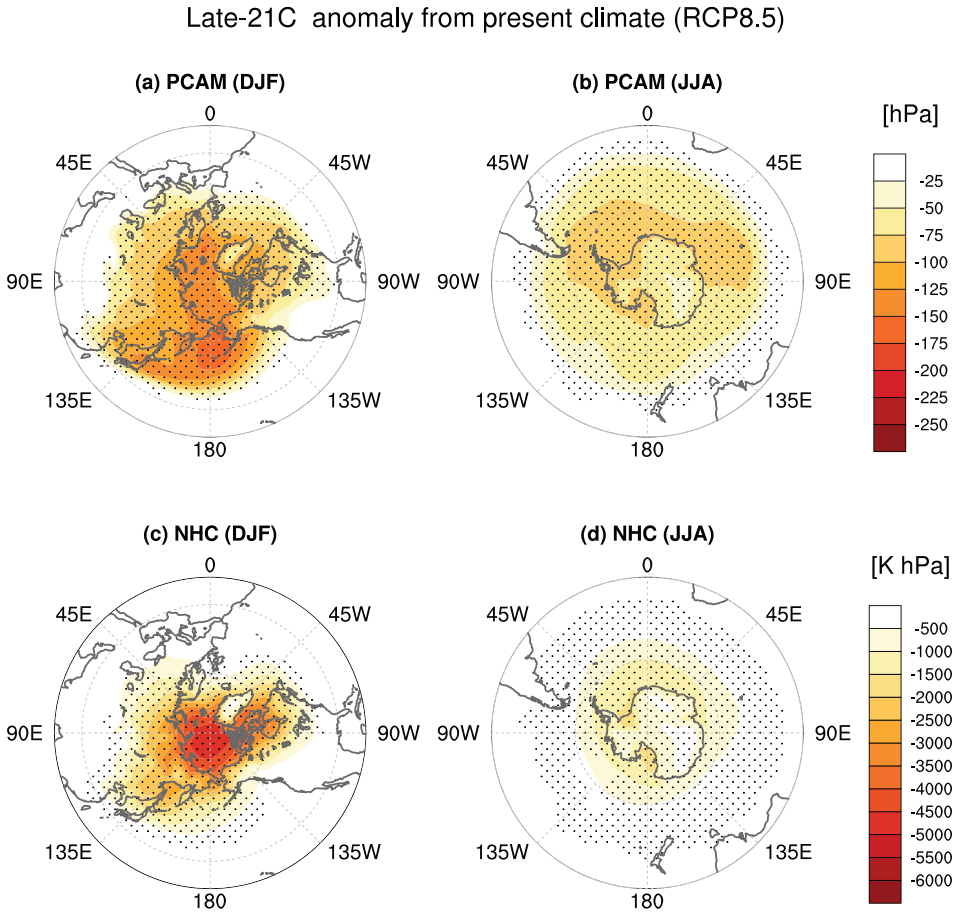

Figure 2. Future changes in (upper panels) the multimodel mean polar cold air mass (PCAM) amount and (bottom panels) negative heat content (NHC) under the RCP8.5 scenario in the late 21st century relative to the present climate. Stippling indicates regions that satisfy the "large change with high model agreement" criteria, whereas hatching indicates regions where the intermodel standard deviation is smaller than the interannual variability.

changes. The multimodel mean of the total hemispheric PCAM amount is projected to decrease by approximately 21% in the NH winter and by approximately 19% in the SH winter under the RCP4.5 scenario in the late 21st century and by approximately 37% in the NH winter and by approximately 34% in the SH winter under the RCP8.5 scenario (Figures 1a and 1b). The multimodel ensemble spread of changes in the PCAM amount under the RCP8.5 scenario is approximately 5% in the mid-21st century and approximately 7% in the late 21st century. The projected multimodel mean reduction in NHC is more than 50% in the NH winter and approximately 40% in the SH winter under the RCP8.5 scenario in the late 21st century (Figures 1c and 1d). Although past decreasing trends were not specified in the SH winter (Kanno et al., 2016), both the PCAM amount and NHC are projected to decrease significantly in the future climate.

Figure 2 shows the spatial patterns of the multimodel mean future changes in the PCAM amount and NHC under the RCP8.5 scenario in the late 21st century, relative to the present climate. In most of the extratropical regions, the decrease in the multimodel mean PCAM amount satisfies the "large change with high model agreement" criteria, indicated by stippling. The PCAM amount decreases greatly in the region from the northern Pacific Ocean to the Arctic Ocean (Figure 2a). In the SH winter, reductions in the PCAM amount are smaller than those in the NH winter. Although all five climate models project a decrease in the PCAM amount in both winters, the changes differ in their magnitudes (Figures S3 and S4). Note that the reductions in the PCAM and NHC are qualitatively the same if the threshold potential temperature is changed by ± 5 K.

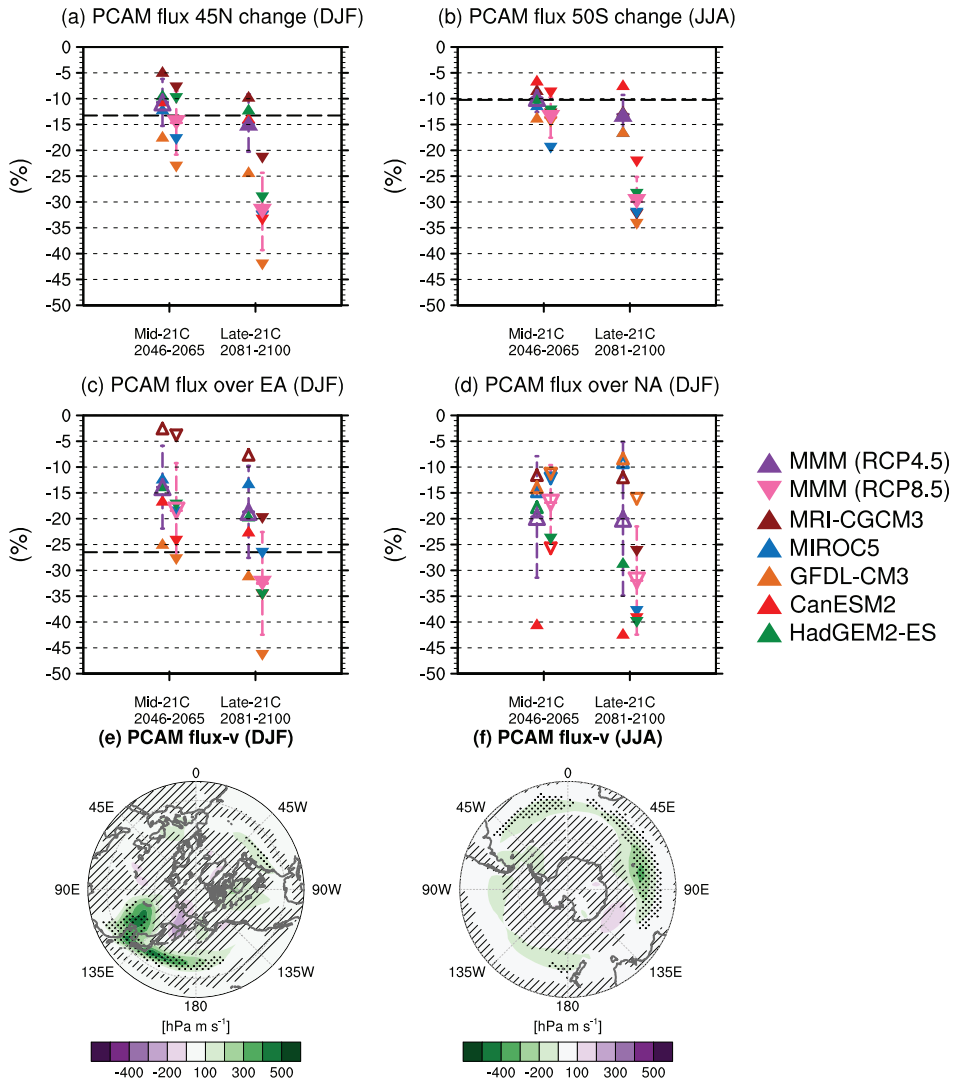

Figure 3. Future changes in the zonally integrated polar cold air mass (PCAM) flux across (a) 45°N, (b) 50°S, (c) 45°N within 90°E–135°E, and (d) 60°N within 80°W–130°W. Changes are relative to the present climate. Filled triangles indicate that changes are statistically significant at the 95% confidence level for each climate model and that changes satisfy the "large change with high agreement" criteria for the multimodel mean. Purple and pink vertical bars represent the widths of the distributions (one standard deviation of the intermodel variability). Black bold broken horizontal lines denote the internal variability (two standard deviations of interannual variability). The internal variability in (d) is 75.4%. Bottom panels show the future changes in the equatorward component of the PCAM fluxes. The bottom left and right panels are the Northern and Southern Hemisphere winters, respectively. The figures show the future changes under the RCP8.5 scenario in the late 21st century relative to the present climate. Stippling indicates regions that satisfy the "large change with high model agreement" criteria, whereas hatching indicates regions where the intermodel standard deviation is smaller than the interannual variability.

As with the PCAM amount, the NHC is projected to decrease in both the NH and SH winters (Figures 2c and 2d). In most of the extratropics, the projected reductions in the NHC satisfy the "large change with high model agreement" criteria. In the NH winter, the multimodel mean as well as each of the individual climate models project the largest reduction in the NHC over the Arctic region (Figures 2c and S5). The magnitude of the reduction is approximately 5,000 K hPa, which corresponds to approximately 80% of the climatological mean NHC (Figure S2c). This is consistent with strong warming in the lower troposphere over the Arctic, as indicated by previous studies (Graversen et al., 2008; Screen & Simmonds, 2010; Wang et al., 2017). The NHC reductions in the SH winter are projected to be relatively small around Antarctica than those around the Arctic in the NH winter.

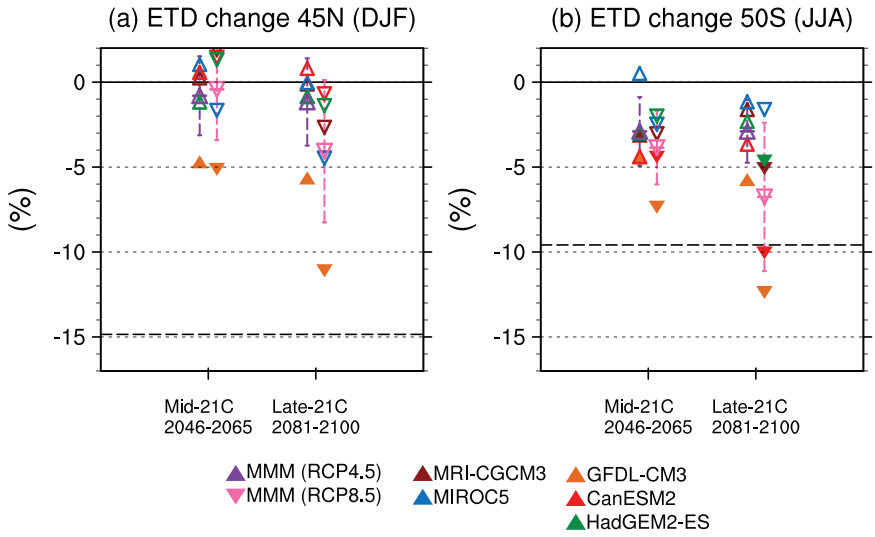

Figure 4. Future changes in the intensity of the extratropical direct (ETD) circulation in the (left) Northern Hemisphere and (right) Southern Hemisphere winters. The ordinate denotes changes relative to their climatological means. Upper (lower) triangles are for RCP4.5 (8.5) scenarios. Filled triangles indicate the changes are significant at the 95% confidence level for each climate model and indicate the "large change with high model agreement" criteria are satisfied for the multimodel mean. Purple and pink vertical bars represent the distribution widths (one standard deviation of the inter-model variability). Black bold broken horizontal lines denote the internal variability (two standard deviations of the interannual variability).

Figures 3a and 3b show the future changes in the equatorward PCAM fluxes across 45°N and 50°S, where the equatorward component of the zonal-mean PCAM fluxes takes its maximum values. In the mid-21st century, the multimodel mean equatorward PCAM fluxes at 45°N decreases by about 10–15% under both of the considered RCP scenarios relative to the present climate. This reduction is comparable with the internal variability of the PCAM fluxes (Figure 3a). This result suggests that CAOs will significantly weaken in the mid-21st century, which is consistent with other modeling studies (Ayarzagüena & Screen, 2016; Chen et al., 2016; Screen, 2017; Sun et al., 2015; Sun et al., 2016). In the late 21st century, the multimodel mean PCAM fluxes decrease by approximately 32% under the RCP8.5 scenario, which exceeds the magnitude of their internal variability. In the SH winter, the reduction in the multimodel mean equatorward PCAM fluxes at 50°S is as large as their internal variability for both RCP scenarios in the mid-21st century. In other words, these reductions become significant around the mid-21st century. In the late 21st century, the multimodel mean PCAM fluxes decrease by approximately 30% compared to the climatological mean values under the RCP8.5 scenario.

Figures 3e and 3f show the geographical distributions of future changes in the equatorward component of the PCAM fluxes in the NH and SH winters, respectively. Note that the equatorward PCAM fluxes indicate the regional CAO activity. All five climate models project large reductions in the equatorward PCAM fluxes from East Asia to the Pacific storm track, an exit region of a major PCAM stream (Figures 3e, S6, and S7), although cold winters have prevailed in recent decades over Siberia (Wang et al., 2017; Cohen, 2018; Ogawa et al., 2018). The reductions are greater than the internal variability there. The multimodel mean shows moderate reductions from central North America to the Atlantic storm track, an exit region of another major PCAM stream (Figure S1), although their statistical significance varies between the climate models (Figures 3e and S7). A comparison of the PCAM flux over East Asia and North America (Figures 3c and 3d) shows that the magnitudes of the weakening are similar between the two regions: approximately 30% for the RCP8.5 scenario at the end of 21st century. However, the large internal variability over North America of 75.4% of the climatology makes it difficult to determine the statistical significance. In addition, weak reductions are found over southeastern Europe. The above three regions are typical regions where intermittent equatorward PCAM fluxes cause severe CAOs (Kanno, Abdillah, et al., 2015). Except for these regions, changes in the equatorward PCAM fluxes are small (denoted by hatching). In the SH winter, the climate models project a decrease in the equatorward PCAM fluxes in the midlatitudes, particularly over

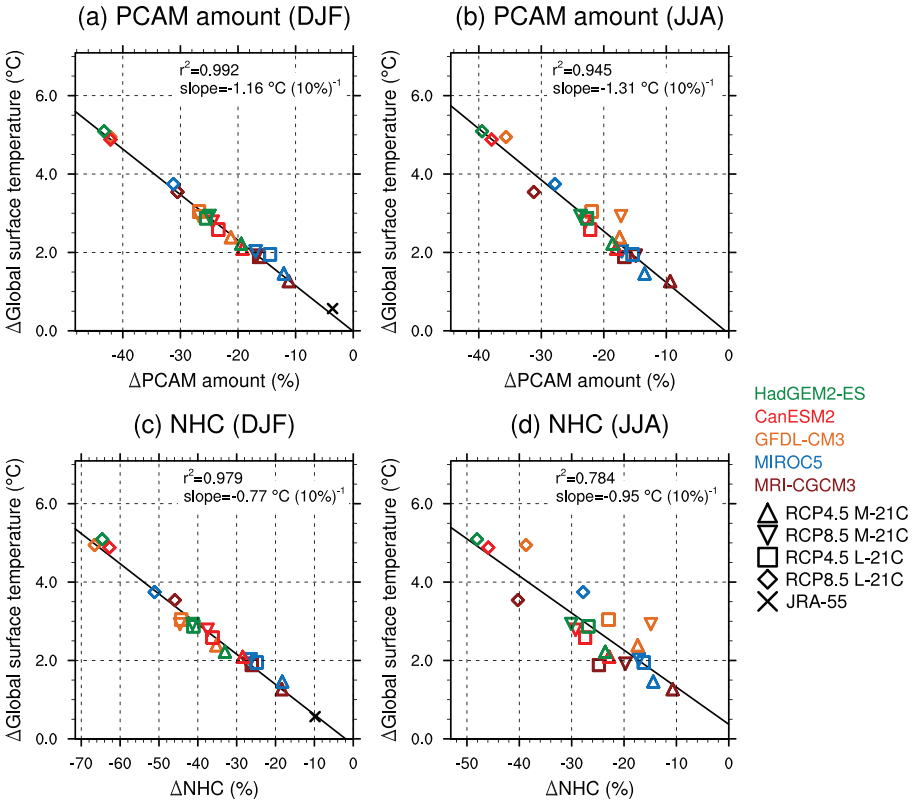

Figure 5. Scatter plots of the global mean surface temperature change against the total hemispheric polar cold air mass (PCAM) amount (upper panels) and negative heat content (NHC) (lower panels). Colors and markers denote the climate models and Representative Concentration Pathway (RCP) scenarios or periods, respectively. Cross marks denote the anomaly between the reference period 1993–2012 and 1959–1978 in the JRA-55 reanalysis data set and are drawn only for the Northern Hemisphere winter. Bold black lines denote the regression slopes. The coefficients of determination and slope coefficient are indicated in each panel.

the southern Atlantic and southern Indian Oceans (Figure 3f). The circumpolar PCAM fluxes are projected to decrease substantially (Figure S6).

Figure 4 shows the future changes in the intensity of the ETD circulation, which indicates the meridional PCAM fluxes with an adjusted threshold potential temperature. Although all future predictions show a weakening of the ETD circulation, their magnitudes are much smaller than the decrease of the PCAM flux below 280 K (Figures 3a and 3b). Under the RCP8.5 scenario in the late 21st century, the multimodel mean decreases by approximately 7% in the NH winter and 9% in the SH winter, which is qualitatively consistent with previous studies (Laliberté & Pauluis, 2010; Wu & Pauluis, 2013). Except for the weakening during the SH winter under the RCP8.5 scenario in the late 21st century, the magnitude of the decrease is smaller than its internal variability. The magnitude of the "upward shift" of the ETD circulation is summarized in Figure S8.

The weakening of the ETD circulation is consistent with the weakening of the wave forcing in the winter hemisphere, indicated by the Eliassen-Palm flux (Figure S9). This dynamical consideration leads to the important conclusion that the weakening of the PCAM fluxes below 280 K can be attributed to two polar warming effects: a large direct effect that reduces the PCAM amount in the high latitudes and a small indirect effect that weakens the ETD circulation. Since the PCAM flux below 280 K decreases by 35% under the RCP8.5 scenario and the ETD circulation by 7%, the contributions of the thermal and dynamical effects are about 80% and 20%, respectively.

Figure 5 shows scatter plots of the global mean surface air temperature increases against the total hemispheric PCAM amount and NHC reductions. The scatter plots clearly show robust linear relationships between the global mean surface air temperature increases and the total hemispheric PCAM amount or

NHC reductions across the future projection scenarios and climate models, with high determination coefficients. The slopes of the regression lines for the PCAM amounts are −1.16 °C per 10% in the NH winter and −1.31 °C per 10% in the SH winter (Figures 5a and 5b). In the NH winter, the linear relationships found in the future changes in the PCAM amount and NHC correspond well with the past changes in the JRA-55 reanalysis for the period 1993–2012 relative to 1959–1978 (Figures 5a and 5c). Miller et al. (2010) found a linear relationship between polar warming and global warming in four different time periods (Last Glacial Maximum, Holocene Thermal Maximum, Last Interglaciation, and Middle Pliocene). The robustness of the linear intermodel relationships suggests that the climate sensitivity has a one-to-one correspondence with the reduction in the total hemispheric PCAM amount. Qualitatively similar results are obtained by using the tropospheric mean temperature instead of the global surface air temperature. The global mean surface air temperature increase does not have a strong relationship with the decrease in the PCAM fluxes, probably due to considerable model dependence (Figure S10).

4. Concluding Remarks

We have quantified changes in the PCAM amount and NHC below a potential temperature of 280 K in climate model output. In the NH winter, the multimodel mean shows a robust reduction in the total hemispheric PCAM amount and NHC of more than 35% and 55% of their climatological means, respectively, under the RCP8.5 scenario in the late 21st century. In the SH winter, the projected reductions are up to 34% in the PCAM amount and 40% in the NHC, although the long-term trends until now were unclear due to large discrepancies among reanalysis data sets (Kanno et al., 2016). Both in the NH and SH winters, increases in the global mean surface air temperature are found to have a robust linear relationship with reductions in the total hemispheric PCAM amount.

The equatorward PCAM fluxes across 45°N and 50°S are projected to weaken in the future climate (Figures 3a and 3b). In the future projections, the magnitude of their reductions becomes comparable to their internal variability in the mid-21st century. It should be noted that in the present climate, the long-term trends are not statistically significant in the NH winter due to its large internal variability (Kanno et al., 2016). Geographically, the extent of the equatorward PCAM fluxes are projected to decrease greatly from East Asia to the Pacific storm track, moderately from the central North America to the Atlantic storm track, and weakly over eastern Europe.

The future changes in the intensity of the ETD circulation, which indicates the PCAM flux with an adjusted threshold potential temperature, leads us to two conclusions. One is that the PCAM fluxes are projected to weaken slightly even if the threshold potential temperature is adjusted. The other is that the weakening of the PCAM fluxes below 280 K is explained by the direct and indirect effects of polar warming. In addition, the magnitude of the upward shift of the ETD circulation gives an indication of the adjustment of the threshold potential temperature in future studies.

Acknowledgments
This research was supported by the Japan Society for the Promotion of Science (JSPS) through a Grant-in-Aid 15H02129 and 18H03738 and through a Grant-in-Aid for Research Fellow (18J01336). The climate model data sets used in this study were downloaded from the ESGF webpage (https://esgf-node.llnl.gov/projects/cmip5/), the JRA-55 reanalysis data sets were downloaded from the JMA data distribution system (http://jra.kishou.go.jp/JRA-55/index_en.html), and ERA-interim from ECMWF (https://apps.ecmwf.int/datasets/data/interim-full-daily/levtype=sfc/). The code for calculation of the isentropic cold air mass metrics is available at http://wind.gp.tohoku.ac.jp/isen_cam/.

References

Abdillah, M. R., Kanno, Y., & Iwasaki, T. (2018). Strong linkage of El Niño-Southern Oscillation to the polar cold air mass in the Northern Hemisphere. *Geophysical Research Letters*, *45*, 5643–5652. https://doi.org/10.1029/2018gl077612

Ayarzagüena, B., & Screen, J. A. (2016). Future Arctic sea ice loss reduces severity of cold air outbreaks in midlatitudes. *Geophysical Research Letters*, *43*, 2801–2809. https://doi.org/10.1002/2016gl068092

Bekryaev, R. V., Polyakov, I. V., & Alexeev, V. A. (2010). Role of polar amplification in long-term surface air temperature variations and modern arctic warming. *Journal of Climate*, *23*(14), 3888–3906. https://doi.org/10.1175/2010jcli3297.1

Chen, H. W., Zhang, F., & Alley, R. B. (2016). The robustness of midlatitude weather pattern changes due to Arctic sea ice loss. *Journal of Climate*, *29*(21), 7831–7849. https://doi.org/10.1175/jcli-d-16-0167.1

Cohen, J. (2018), Arctic change and possible influence on mid-latitude climate and weather: A US CLIVAR white paper Rep. https://doi.org/10.5065/D6TH8KGW

Gao, Y., Leung, L. R., Lu, J., & Masato, G. (2015). Persistent cold air outbreaks over North America in a warming climate. *Environmental Research Letters*, *10*, 044001. https://doi.org/10.1088/1748-9326/10/4/044001

Graversen, R. G., Mauritsen, T., Tjernstrom, M., Kallen, E., & Svensson, G. (2008). Vertical structure of recent Arctic warming. *Nature*, *451*(7174), 53–56. https://doi.org/10.1038/nature06502

Hankes, I. E., & Walsh, J. E. (2011). Characteristics of extreme cold air masses over the North American sub-Arctic. *Journal of Geophysical Research*, *116*, D11102. https://doi.org/10.1029/2009jd013582

Holland, M. M., & Bitz, C. M. (2003). Polar amplification of climate change in coupled models. *Climate Dynamics*, *21*(3-4), 221–232. https://doi.org/10.1007/s00382-003-0332-6

IPCC (2013). *Climate change 2013: The physical science basis. Contribution of Working Group I to the Fifth Assessment Report of the Intergovernmental Panel on Climate Change.* Cambridge, United Kingdom and New York, NY, USA: Cambridge University Press.

Iwasaki, T., Shoji, T., Kanno, Y., Sawada, M., Ujiie, M., & Takaya, K. (2014). Isentropic analysis of polar cold airmass streams in the Northern Hemispheric winter. *Journal of the Atmospheric Sciences*, *71*(6), 2230–2243. https://doi.org/10.1175/Jas-D-13-058.1

Kanno, Y., Abdillah, M. R., & Iwasaki, T. (2015). Charge and discharge of polar cold air mass in Northern Hemispheric winter. *Geophysical Research Letters*, *42*, 7187–7193. https://doi.org/10.1002/2015gl065626

Kanno, Y., Abdillah, M. R., & Iwasaki, T. (2016). Long-term trend of cold air mass amount below a designated potential temperature in Northern and Southern Hemispheric winters using reanalysis data sets. *Journal of Geophysical Research: Atmospheres*, *121*, 10,138–10,152. https://doi.org/10.1002/2015jd024635

Kanno, Y., Shoji, T., & Iwasaki, T. (2015). Comparison study of the polar cold air mass between Northern and Southern Hemispheric winters based on a zonal-mean two-box model. *Atmospheric Science Letters*, *16*(1), 70–76. https://doi.org/10.1002/asl2.522

Kanno, Y., Walsh, J. E., Abdillah, M. R., Yamaguchi, J., & Iwasaki, T. (2019). Indicators and trends of polar cold airmass. *Environmental Research Letters*, *14*, 025006. https://doi.org/10.1088/1748-9326/aaf42b

Kanno, Y., Walsh, J. E., & Iwasaki, T. (2017). Interannual variability of the North American cold air stream and associated synoptic circulations. *Journal of Climate*, *30*(23), 9575–9590. https://doi.org/10.1175/Jcli-D-17-0104.1

Kay, J. E., Holland, M. M., Bitz, C. M., Blanchard-Wrigglesworth, E., Gettelman, A., Conley, A., & Bailey, D. (2012). The influence of local feedbacks and northward heat transport on the equilibrium Arctic climate response to increased greenhouse gas forcing. *Journal of Climate*, *25*(16), 5433–5450. https://doi.org/10.1175/jcli-d-11-00622.1

Kodra, E., Steinhaeuser, K., & Ganguly, A. R. (2011). Persisting cold extremes under 21st-century warming scenarios. *Geophysical Research Letters*, *38*, L08705. https://doi.org/10.1029/2011gl047103

Laliberté, F., & Pauluis, O. (2010). Winter intensification of the moist branch of the circulation in simulations of 21st century climate. *Geophysical Research Letters*, *37*, L20707. https://doi.org/10.1029/2010gl045007

Landgren, O. A., Seierstad, I. A., & Iversen, T. (2019). Projected future changes in marine cold-air outbreaks associated with polar lows in the northern North-Atlantic Ocean. *Climate Dynamics*, *53*(5-6), 2573–2585. https://doi.org/10.1007/s00382-019-04642-2

Martin, J. E. (2015). Contraction of the Northern Hemisphere, lower-tropospheric, wintertime cold pool over the past 66 years. *Journal of Climate*, *28*(9), 3764–3778. https://doi.org/10.1175/jcli-d-14-00496.1

Miller, G. H., Alley, R. B., Brigham-Grette, J., Fitzpatrick, J. J., Polyak, L., Serreze, M. C., & White, J. W. C. (2010). Arctic amplification: Can the past constrain the future? *Quaternary Science Reviews*, *29*(15–16), 1779–1790. https://doi.org/10.1016/j.quascirev.2010.02.008

Ogawa, F., Keenlyside, N., Gao, Y., Koenigk, T., Yang, S., Suo, L., et al. (2018). Evaluating impacts of recent Arctic sea-ice loss on the northern hemisphere winter climate change. *Geophysical Research Letters*, *45*, 3255–3263. https://doi.org/10.1002/2017gl076502

Park, T. W., Ho, C. H., Jeong, S. J., Choi, Y. S., Park, S. K., & Song, C. K. (2011). Different characteristics of cold day and cold surge frequency over East Asia in a global warming situation. *Journal of Geophysical Research*, *116*, D12118. https://doi.org/10.1029/2010jd015369

Peings, Y., Cattiaux, J., & Douville, H. (2012). Evaluation and response of winter cold spells over Western Europe in CMIP5 models. *Climate Dynamics*, *41*(11-12), 3025–3037. https://doi.org/10.1007/s00382-012-1565-z

Sasai, T., Kawase, H., Kanno, Y., Yamaguchi, J., Sugimoto, S., Yamazaki, T., et al. (2019). Future projection of extreme heavy snowfall events with a 5-km large ensemble regional climate simulation. *Journal of Geophysical Research: Atmospheres*. https://doi.org/10.1029/2019JD030781

Screen, J. A. (2017). Simulated atmospheric response to regional and pan-Arctic sea ice loss. *Journal of Climate*, *30*(11), 3945–3962. https://doi.org/10.1175/jcli-d-16-0197.1

Screen, J. A., & Simmonds, I. (2010). The central role of diminishing sea ice in recent Arctic temperature amplification. *Nature*, *464*(7293), 1334–1337. https://doi.org/10.1038/nature09051

Serreze, M. C., Barrett, A. P., Stroeve, J. C., Kindig, D. N., & Holland, M. M. (2009). The emergence of surface-based Arctic amplification. *The Cryosphere*, *3*(1), 11–19. https://doi.org/10.5194/tc-3-11-2009

Shoji, T., Kanno, Y., Iwasaki, T., & Takaya, K. (2014). An isentropic analysis of the temporal evolution of East Asian cold air outbreaks. *Journal of Climate*, *27*(24), 9337–9348. https://doi.org/10.1175/Jcli-D-14-00307.1

Steig, E. J., Schneider, D. P., Rutherford, S. D., Mann, M. E., Comiso, J. C., & Shindell, D. T. (2009). Warming of the Antarctic ice-sheet surface since the 1957 International Geophysical Year. *Nature*, *457*(7228), 459–462. https://doi.org/10.1038/nature07669

Sun, L., Deser, C., & Tomas, R. A. (2015). Mechanisms of stratospheric and tropospheric circulation response to projected Arctic sea ice loss. *Journal of Climate*, *28*(19), 7824–7845. https://doi.org/10.1175/jcli-d-15-0169.1

Sun, L., Perlwitz, J., & Hoerling, M. (2016). What caused the recent "warm Arctic, cold continents" trend pattern in winter temperatures? *Geophysical Research Letters*, *43*, 5345–5352. https://doi.org/10.1002/2016gl069024

Taylor, K. E., Stouffer, R. J., & Meehl, G. A. (2012). An Overview of CMIP5 and the experiment design. *Bulletin of the American Meteorological Society*, *93*(4), 485–498. https://doi.org/10.1175/Bams-D-11-00094.1

Vavrus, S., Walsh, J. E., Chapman, W. L., & Portis, D. (2006). The behavior of extreme cold air outbreaks under greenhouse warming. *International Journal of Climatology*, *26*(9), 1133–1147. https://doi.org/10.1002/joc.1301

Wang, S. Y. S., Lin, Y.-H., Lee, M.-Y., Yoon, J.-H., Meyer, J. D. D., & Rasch, P. J. (2017). Accelerated increase in the Arctic tropospheric warming events surpassing stratospheric warming events during winter. *Geophysical Research Letters*, *44*, 3806–3815. https://doi.org/10.1002/2017gl073012

Wu, Y., & Pauluis, O. (2013). Examination of isentropic circulation response to a doubling of carbon dioxide using statistical transformed Eulerian mean*. *Journal of the Atmospheric Sciences*, *70*(6), 1649–1667. https://doi.org/10.1175/jas-d-12-0235.1

Zhang, Y., Sperber, K. R., & Boyle, J. S. (1997). Climatology and interannual variation of the East Asian winter monsoon: Results from the 1979-95 NCEP/NCAR reanalysis. *Monthly Weather Review*, *125*(10), 2605–2619. https://doi.org/10.1175/1520-0493(1997)125<2605:Caivot>2.0.Co;2